Cellulose nano-crystals as a sensitive and selective layer for high performance surface acoustic wave HCl gas sensors

Yongliang Tang[1*], Xiaofeng Xu[2], Huarong Du[1], Hao Zhu[1], Dengji Li[2], Dongyi Ao[2], Yuanjun Guo[2], YongQing Fu[3], Xiaotao Zu[2]

[1]School of Physical Science and Technology, Southwest Jiaotong University, Chengdu, 610031, P. R. China.

[2]School of Physics, University of Electronic Science and Technology of China, Chengdu, 610054, P. R. China.

[3]Faculty of Engineering and Environment, Northumbria University, Newcastle upon Tyne, NE1 8ST, UK

[*]Correspondence Author:

Yongliang Tang :E-mail address: tyl@swjtu.edu.cn; Telephone: +86-15884573263

Abstract

We report that cellulose nano-crystals (CNCs) can be used as a sensitive and selective layer in surface acoustic wave (SAW) sensors for in-situ HCl gas detection. CNCs were prepared through directly hydrolysis of cotton fiber and were spin-coated on quartz SAW resonators to form the sensitive layer. The CNCs have been identified to have abundant hydroxyl groups on their surfaces, which can act as the perfect adsorption sites for H_2O, which can further act as the active sites for HCl gas adsorption. The absorption of HCl on the CNCs layer, thus leads to an increase of its mass, causing negative responses of the SAW sensors. Ambient humidity and thickness of CNCs layer are found to have significant influences on the responses of the SAW sensor. With an 80-nm-thick CNCs layer, the sensor shows a response of -2 kHz to 1 ppm HCl at 25 °C and relative humidity of 50% with an excellent selectivity and recovery characteristics.

Keywords: SAW; HCl sensor; cellulose nano-crystal; hydroxyl groups; H_2O

1. introduction

Long-term health of living organisms is highly dependent on the ambient environment [1-4]. However, the deterioration of environment, especially due to the air pollution, has accelerated significantly in the past decades [5-8]. There are various types of air pollutants including hazardous gases, dusts, and toxic smoke. Among these pollutants, hazardous gases are highly harmful, which can cause various diseases, cancer and even death [9-11]. One of the most dangerous hazardous gases is hydro-chloride (HCl), which is commonly produced from chemical, metallurgical, pharmaceutical industries, or waste incineration. HCl can acidify soil and water, and also damage or even kill plants. Moreover, it can damage the skins, mucosa of eyes and noses of human beings and animals [12-14]. The standard from Occupational Safety and Health Administration defines the Immediately Dangerous to Life or Health concentrations of HCl are 50 ppm and 5 ppm, respectively [15]. Therefore, it is necessary to develop highly sensitive HCl sensors for early detection and continuous monitoring of its leakage in order to counter the accidental threats.

In the past decades, electrochemical, gas chromatographic, opto-chemical and optical HCl gas sensors have been developed [16-21]. However, these sensors are generally time consuming, or their sensitivities are not good, or expensive instrumentation [20]. Therefore, there is an urgent need for highly sensitive and selective sensors for rapid and in situ detection of HCl. To achieve this goal, mass-sensitive sensors based on quartz crystal microbalance (QCM) and surface acoustic wave (SAW) techniques are possible solutions. Recently, QCM HCl sensors with excellent sensitivity have been reported already [20, 22-24]. However, few reports are focused on SAW sensors, which should have higher sensitivity than QCM because of their higher working frequency [25-27].

The SAW sensors are highly sensitive to the extremely tiny mass changes of its sensitive layer materials deposited on the surface of SAW devices [28-30]. Hence, with using a sensitive material which can effectively and selectively absorb HCl from the ambient environment, the SAW sensor will be highly sensitive to HCl gas. Cellulose nano-crystal (CNC), a promising material derived from naturally occurring cellulose, was already applied in various fields such as catalysis, energy and electronic devices, biomedical devices, wastewater treatment and so on [31-35]. CNC has various exceptional characteristics such as large specific surface area (~ 250 m^2/g) and abundant surface hydroxyl groups, which are beneficial for the gas sensing [36,37], especially for the HCl gas sensing. It has been reported that surface hydroxyl groups on the CNCs can act as the active sites to absorb H_2O by forming hydrogen bonds, making the CNCs always partially covered with water molecules in the ambient environment [38]. The adsorbed H_2O molecules may easily capture the HCl in the ambient environment because of the superior solubility of HCl in H_2O. The captured HCl leads to an increase of the mass of the CNCs, and finally results in the significant responses of the sensor. Therefore, it can be speculated that the CNCs could be explored as a good sensing material for SAW HCl sensors.

In this article, we fabricated a sensitive SAW HCl gas sensor with the CNCs as the sensitive layer. The responses, defined as shifts of oscillating frequency of the sensor, are ~-2 and -10 kHz to 1 and 5 ppm HCl gases, respectively. The sensing mechanisms were systematically studied, and the changes of mass of the CNC_S layer were found to contribute to SAW signal responses. In addition, the ambient humidity and thickness of the layer were found highly affecting the responses of the sensor. The ambient temperature may also affect the responses. However, a study of temperature effects was not conducted because it is beyond the scope of this work.

2. Experimental details

2.1 Preparation of SAW resonator and sensitive layers on SAW resonators

The SAW resonator with a central frequency of 200 MHz was based on a ST-cut quartz substrate. It consists of 30 pairs of input and output interdigital transducers (IDTs) and 100 pairs of reflection gratings on each end of the quartz substrate. The IDTs and reflection gratings with a periodicity of 16 μm were fabricated by the conventional lithography technique on a 200 nm thick Al thin film deposited by magnetron sputtering. The aperture of the IDTs is 3 mm.

The CNCs were prepared through sulfuric acid hydrolysis of cotton powder based on a previously published protocol [39,40]. Briefly, 10 g cotton powder (Whatman) was hydrolyzed in 200 ml 64 wt% sulfuric acid (Chengdu Kelong) at 45 °C under a vigorous agitation for 1 hour to obtain a cellulose suspension, which was then diluted with 2L deionized water. After ~2 hrs, the clear top layer of the diluted suspension was decanted. The suspension left was repeatedly concentrated and washed by centrifugation until the supernatant appeared turbid. The obtained suspension was dialyzed against slow running deionized distilled water until the effluent was remained with a neutral pH value. The solid aggregates in the suspension were agitated ultrasonically for 2 hrs in an ice bath to create the CNCs colloidal suspension, which was kept over ion-exchange resin for 7 days and then filtered through filter paper.

For preparation of CNCs sensitive layers on SAW resonators, the obtained CNCs suspension was diluted with deionized water to obtain a suspension with a concentration of 2 mg/ml under a vigorous agitation using a cantilever agitator working at 6000 rpm. This diluted suspension was coated onto the SAW resonator

using a spin-coating method with a speed of 5000 rpm for 30 s, and the thickness of CNCs layers can be adjusted by varying the coating cycles. The synthesized CNCs layers were designated according to the coating procedure. For example, the CNCs layer obtained through 3 spin-coating cycles was designated as CNCs-3.

To compare the performance of the CNCs as the sensing layer for HCl detection when humidity is changing, graphene oxide (GO) and SiO_2 layers were also prepared. For preparation of the GO layer on the SAW resonator, the GO suspension (2 mg/ml, obtained from XFnano) was directly spin-coated onto a SAW resonator with a speed of 5000 r/min for 30 s for 4 cycles. For preparation of the SiO_2 layer, the SiO_2 sol was prepared using the Stober method as described in our previous report [41] and was directly spin-coated onto the SAW resonator with a speed of 5000 r/min for 30 s.

For their optimized performance, the CNCs and GO coated SAW resonators were put into an oven at 60 °C for 2 hrs to remove any excess water on the layers. The SiO_2 coated SAW resonator was put into a muffle furnace at 300 °C for 1 h.

For the fabrication of the SAW gas sensor, SAW resonators coated with sensitive layers were connected to a peripheral matching circuit including a cascade amplifier to build SAW oscillators, as shown in Figs. 1(a) and 1(b).

2.2 Material characterization and gas sensing set-up

A Rigaku D/max-2400 X-ray diffractometer was employed to characterize the crystallinity of prepared sensing layers. A field-emission scanning electron microscope (SEM, FEI Inspect F) was used to characterize the morphology of the prepared layers. A Fourier Transform Infrared spectroscopy (FTIR, Nicolet IS 10, with a wavelength range of 400–4000 cm^{-1}) was used to collect the infrared

transmission spectra of prepared layers, and the chemical elemental binding information was obtained using an X-ray photoemission spectroscope (XPS, Kratos Axis Ultra DLD, Al Kα radiation).

The experimental setup for gas sensing measurement system is shown in Fig. 1(b). During the measurement, the ambient temperature was kept at 25 °C. The SAW sensor was placed inside a test chamber. Certified gas cylinders of low concentration test gases (2%, balanced in synthetic dry air) including (HCl, NH_3, SO_2, NO_2, H_2S, CO, H_2, CH_4), together with a gas delivery system employing a mass flow controller and a humidity generator, were used to control the concentration of test gases and the humidity in the test chamber. The oscillating frequency of the SAW sensor was recorded using a frequency counter. The response of the SAW sensor was defined as $\Delta f = f_s - f_0$, where f_s is the working frequency of the sensor with exposure to the test gas, and f_0 is the working frequency in the pure air, respectively. For the measurement of the frequency responses, pure humid or dry air was firstly introduced into the chamber. When the relative humidity in the chamber reached a constant value, the test gas was introduced, and the response of the sensor happened. When the response of the sensor reached a stable value, the test gas was shut off to allow the sensor to recover to its initial state. The response and recovery times are defined as the time taken for the sensor to achieve 90% of the total frequency shift in the cases of response and recovery processes, respectively.

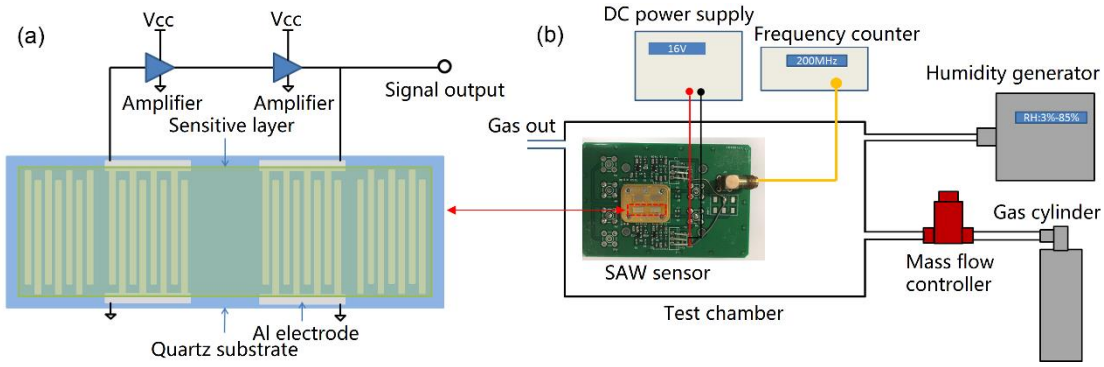

Figure 1 (a) The schematic diagram of a SAW sensor and (b) experimental setup for gas sensing measurement.

3. Results and discussion

3.1 Structural characterization

Fig. 2(a) shows the X-ray diffraction pattern of the CNCs layer. There are three typical diffraction peaks of cellulose crystals centered at 16.5°, 22.5° and 34.5°, corresponding to the (110), (200), and (004) reflection planes of the cellulose I structure [42]. The crystallinity index of the CNCs estimated according to Segal equation [43] is ~67%. Crystal sizes of (110) and (200) planes of the CNCs samples were estimated to be 2.9 and 4.5 nm, respectively, according to the Scherrer equation.

XPS results of the CNCs are shown in Figs. 2(b) and 2(c). The carbon/oxygen atomic ratio obtained from XPS analysis is ~1.34. The high resolution C1s peak of the CNCs (Fig. 2(b)) consists of three different components which can be deconvoluted into: C-C/C-H in aromatic rings (284.7 eV); C-OH (286.2 eV); C-O-C/C=O (287.3 eV) [44]. The relative ratio of C-OH estimated from the peak area is ~43%. Fig. 2(c) presents the high resolution O1s spectrum, which can be deconvoluted into: C-OH (531.5 eV) and C-O-C (532.7 eV) [45], and the estimated C-OH ratio is ~42%. These results indicate that there are a large amount of hydroxyl groups on the CNCs.

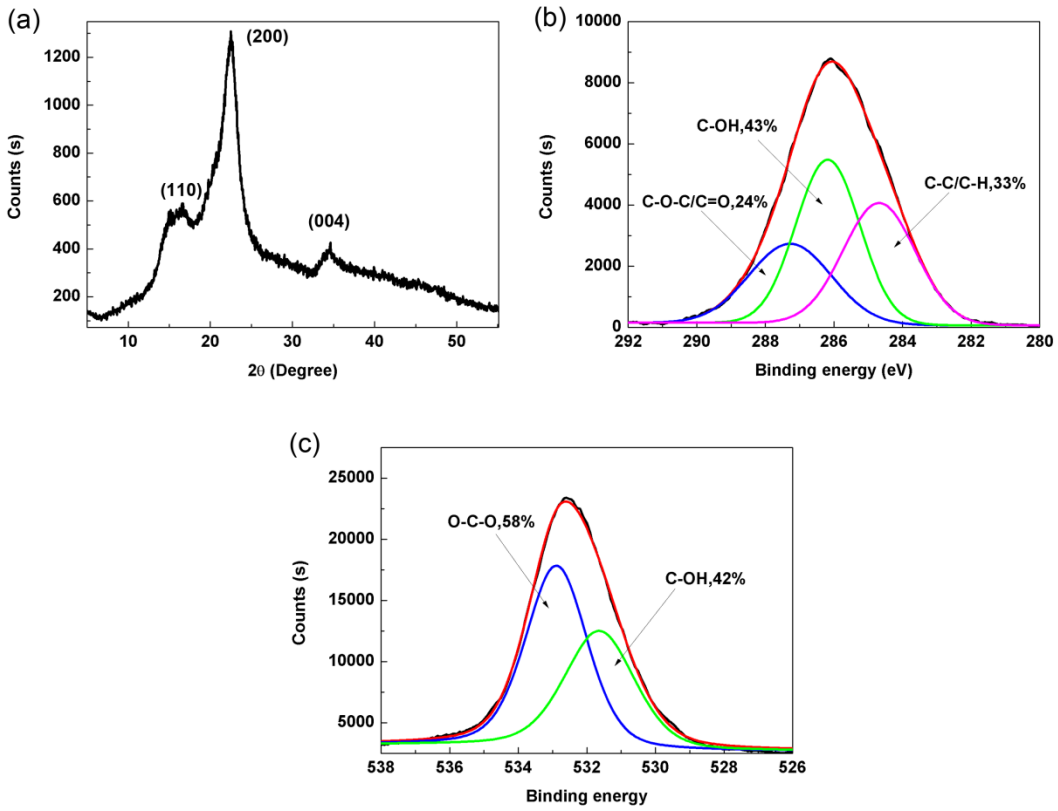

Figure 2 (a) X-ray diffraction pattern of the prepared CNCs layer; (b) C1s XPS spectra and (c) O1s XPS spectra collected on prepared CNCs layer.

Figs. 3(a) and 3(b) show SEM images of surface morphology of the CNCs layer. As shown, the layer is consisted with grainy structures with a diameter of ~20 nm and a length of ~200 nm. This layer is also quite porous. The brighter nano-particles shown in Fig. 3(b) are Au, which were deposited for the SEM characterization (because CNCs are insulating materials). The inset images in Fig. 3(b) present the cross-sectional images of the CNCs-1, CNCs-2 and CNCs-3 layers, indicating the thicknesses of these three layers are ~30, 50 and 80 nm, respectively.

Figs. 3(c) and 3(d) are SEM images of GO and SiO_2 layers which were used for comparisons of sensing layer performance. The GO layer has a crumpled morphology,

and the inset image indicates its thickness is ~80 nm. The SiO_2 layer with a thickness of ~80 nm shows a porous structure, which consists of nano-particles with a diameter of 20 nm.

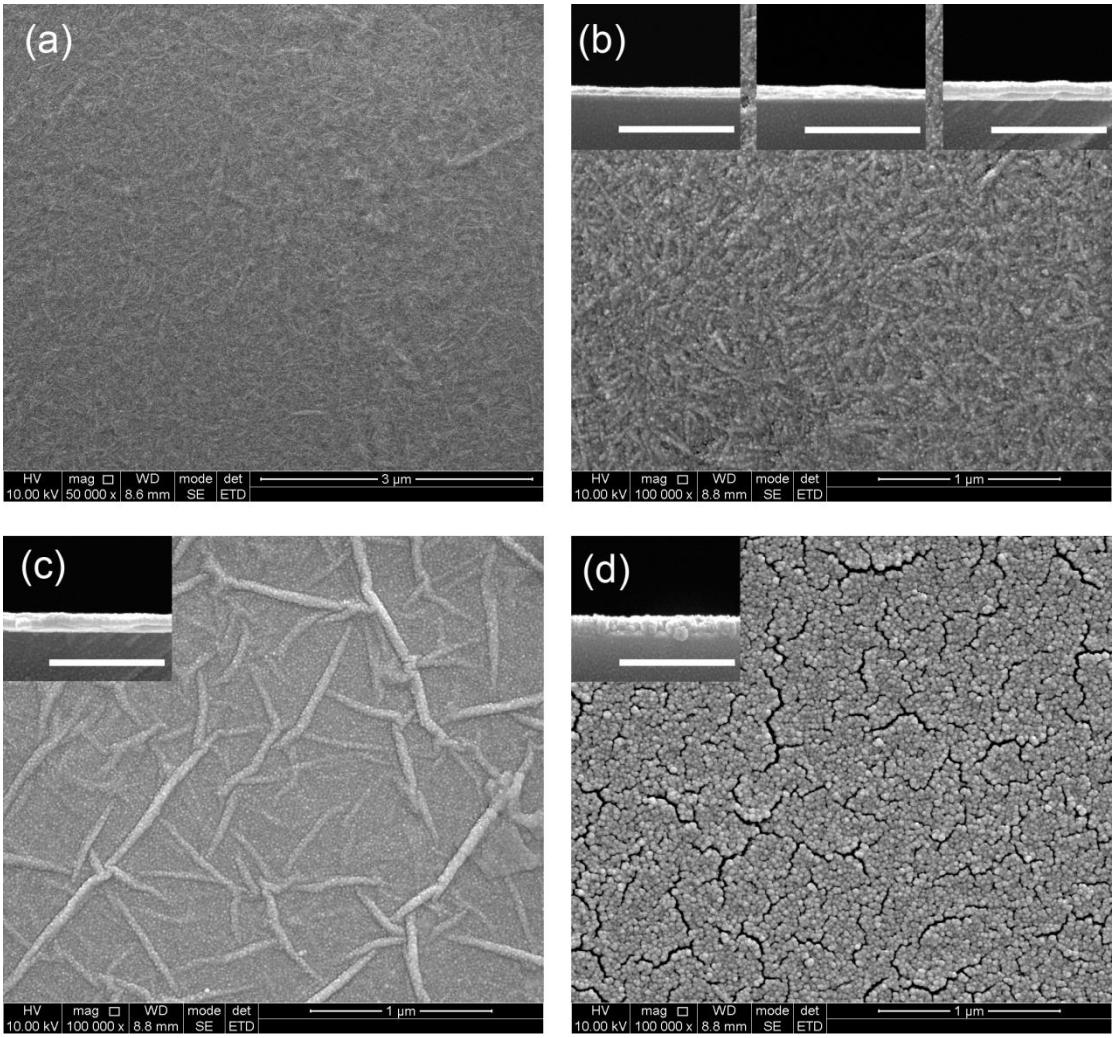

Figure 3 (a) and (b) SEM images of CNCs layers deposited on SAW resonators, the inset images in (b) present the cross-sectional morphologies of CNCs-1 (left), CNCs-2 (middle) and CNCs-3 (right). SEM images of (c) GO and (d) SiO_2 layers deposited on SAW resonators. The scale bars in inset pictures are 500 nm.

FTIR result of CNCs layers is shown in Fig. 4. The strong and broad peak in the range of 3700-3000 cm^{-1} is identified as the -OH stretching vibration of absorbed water molecules, and the peak centered at 1630 cm^{-1} can be assigned as the -OH bending vibration of absorbed water molecules [40]. The C-H stretching vibration and $-CH_2-(C_6)-$ bending vibration has a peak around 2900 and 1430 cm^{-1} respectively, while the deformation, wagging and twisting modes of the anhydroglucopyranose unit are observed from 1800 to 600 cm^{-1} based on the literature [40]. The FTIR results together with the XPS results indicate clearly that there are abundant water molecules absorbed on the CNCs layer due to the formation of hydrogen bonds connecting between the hydroxyl groups and water molecules. FTIR results of the GO and SiO_2 layers are also shown in Fig. 4. Both of these two spectra exhibit similar peaks which can be assigned as -OH stretching and bending vibrations of absorbed water molecules, indicating that there are also abundant absorbed water molecules on these two layers.

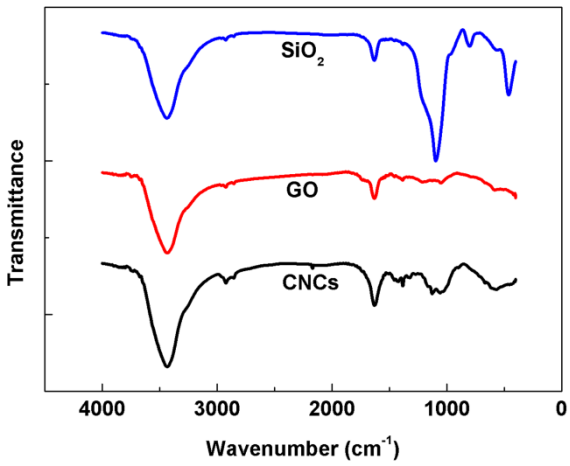

Figure 4 FTIR results of the CNCs, GO and SiO_2 layers coated on SAW resonators

3.2 Sensing performance and mechanisms

Fig. 5 shows the sensing performance of the SAW sensors with and without CNCs sensitive layers tested at 25 °C and RH=50%. The sensors with the CNCs layers exhibited significant negative frequency shifts (~-4, -6.5, and -10 KHz) after they were exposed to 5 ppm HCl gas, but showed a full recovery to its initial state when the HCl was released. On the contrary, the SAW sensor without this sensitive layer showed a slight frequency shift of ~-200 Hz. This result clearly indicates that the CNCs layer significantly enhance the sensitivity of the HCl sensor.

It is well-known that the frequency shift of SAW gas sensors is mainly due to the changes of electric conductivity (electric loading effect), elastic modulus (elastic loading effect), and mass (mass loading effect) of the sensitive layer, caused by the interactions between the sensitive layer and the test gas [46-48]. In this study, the CNCs sensing layer is insulating, and the previous work has revealed that the electric loading effect can be neglected for an insulating layer [48]. Therefore, the negative response of our sensor is probably due to either elastic changes or mass loading effects, as it is well-known that both an increase in mass and a decrease in elastic modulus of the CNCs layer can lead to negative frequency shifts [46-48]. In order to investigate which is the dominant factor for the frequency changes, the influence of the thickness of the CNCs layer on the response was investigated. As show in Fig. 5(b), responses of sensors are enhanced linearly with the increased thickness of the CNCs layer, and can reach ~-10 KHz when the thickness is ~80 nm. Fig. 5(c) also shows that the response (~45 s) and recovery (~500 s) times are almost the same for these sensors.

The relationship between the response (Δf) and the changes of mass and elastic modulus of the sensitive layer follows the equation below [46,47],

$$\Delta f = -c_m f_0^2 \Delta\rho_s + c_e f_0^2 h\Delta\left[\frac{4\mu}{v_0^2}\left(\frac{\lambda+\mu}{\lambda+2\mu}\right)\right] \quad (1)$$

where λ and μ are the shear and bulk modulus of elasticity, c_m and c_e are the sensitivity coefficients of mass and elasticity respectively, h is the thickness of the CNCs sensing film and ρ_s is the density per unit area of the sensing film. v_0 is the unperturbed velocity of the SAW sensor, f_0 is the fundamental frequency of the SAW sensor. According to Equ. (1), it can be concluded that the change of mass of the sensitive layer has a linear relationship with the response of the SAW sensor, whereas the changes of the elastic modulus is not linearly related with the response. Our experimental results have revealed that the responses of the SAW sensors to HCl gas are linearly related with the increased thickness of the CNCs layer (Fig. 5(b)). Therefore, it can be speculated that the microstructure (density, porosity, pore size, specific surface area etc.) of the CNCs layers of different thicknesses kept the same, i.e., the elastic moduli of layers kept the same. Only in this circumstance, the amount of the HCl gas molecules adsorbed by the CNCs layers would increase linearly with the increased thickness of the layer. As a result, the increased mass of the CNCs layers caused by the adsorbed HCl molecules is linearly related to the increased thickness of the CNCs layer. Based on above discussion, the increase of mass should be the major contribution to the frequency response.

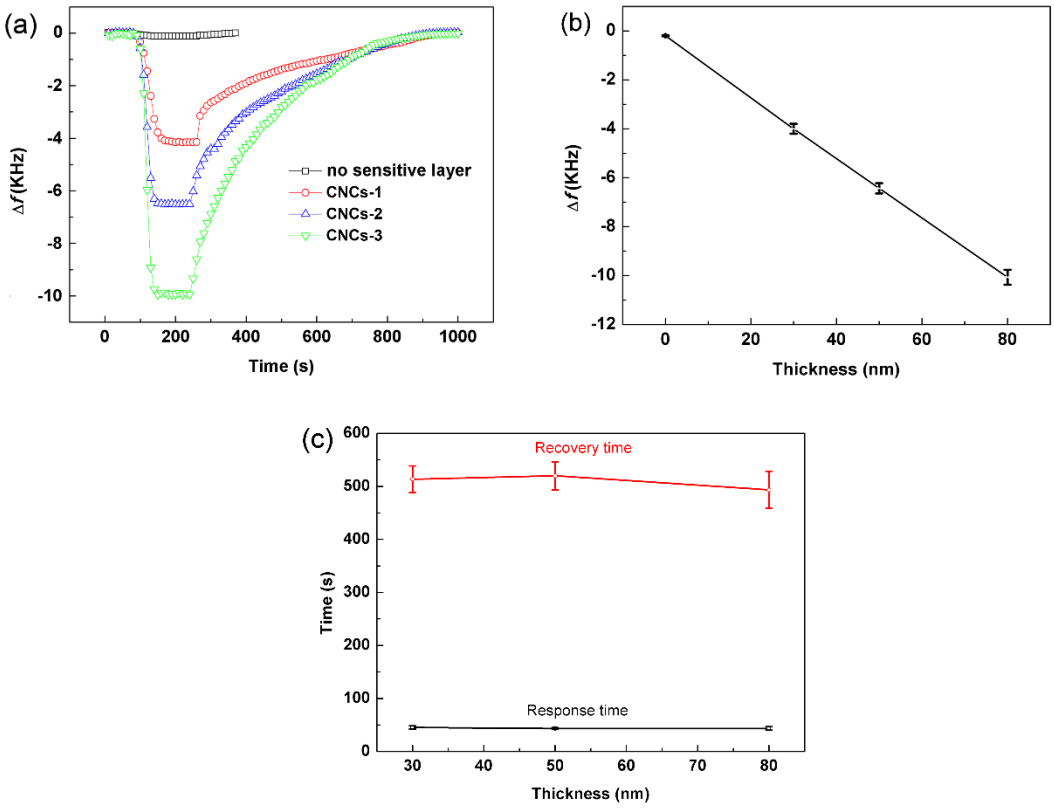

Figure 5 (a) Dynamic responses of the sensors of CNCs-1, CNCs-2, CNCs-3 and without sensitive layer to 5 ppm HCl gas; (b) Responses of sensors as a function of the thickness of the CNCs sensitive layer; (c) Responses and recovery times of sensors as a function of the thickness of the CNCs sensitive layer. All the data are acquired at 25 °C and RH=50%.

The increase of mass of CNCs layers is mainly due to the adsorption of the HCl gas molecules. When CNCs layers are exposed to HCl gas, two potential adsorption processes would happen (see Fig. 6). XPS results have revealed that there are abundant hydrophilic hydroxyl groups on the surface of CNCs layer, and these hydroxyl groups can capture a large amount of H_2O molecules from ambient environment by formation of hydrogen bonds, as confirmed by FTIR result. As shown

in Fig. 6, in the process (1), these captured H_2O molecules act as active sites for HCl adsorption because of the superior solubility of HCl in H_2O, making the CNCs layer much heavier. In the process (2), the hydroxyl groups themselves may capture HCl. Obviously, this process can also lead to an increase on the mass of the CNCs layer.

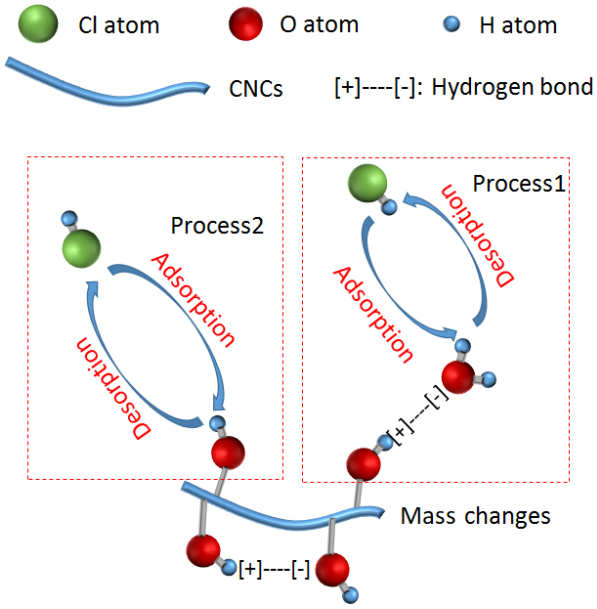

Figure 6 Proposed HCl adsorption and desorption processes on CNCs layer.

Both processes (1) and (2) may be responsible for negative responses of sensors. To verify which process is more dominant, the sensor coated with CNCs-3 layer was tested under different RH values of 3%, 30%, 50% and 85%. As shown in Figs. 7(a) and 7(b), the sensor does not show significant responses to 5 ppm HCl gas under RH=3%. However, with the increase of the RH value, the sensor's responses to the HCl gas is enhanced significantly, and can reach up to ~-22 KHz when RH=85% (Fig. 7(b)). Higher RH values may result in more H_2O molecules absorbed on the CNCs layer. To verify this, the frequency shifts of the sensor were also recorded when the RH value was changed. As shown in Fig. 7(a), the frequency shifts are -32, -96 and -191 KHz when the RH values are increased from 3% to 30%, from 3% to 50% and

from 3% to 85%, respectively. This result confirms that the CNCs layer is highly hydrophilic and there are more H_2O molecules absorbed on the layer at higher RH values according to ref. [46-48]. With more H_2O absorbed, obviously the process (1) will be enhanced significantly, whereas the process (2) will become weaker since more hydroxyl groups are occupied by H_2O molecules. Hence, it can be concluded that the process (1) shall make the major contribution to the responses of the sensor.

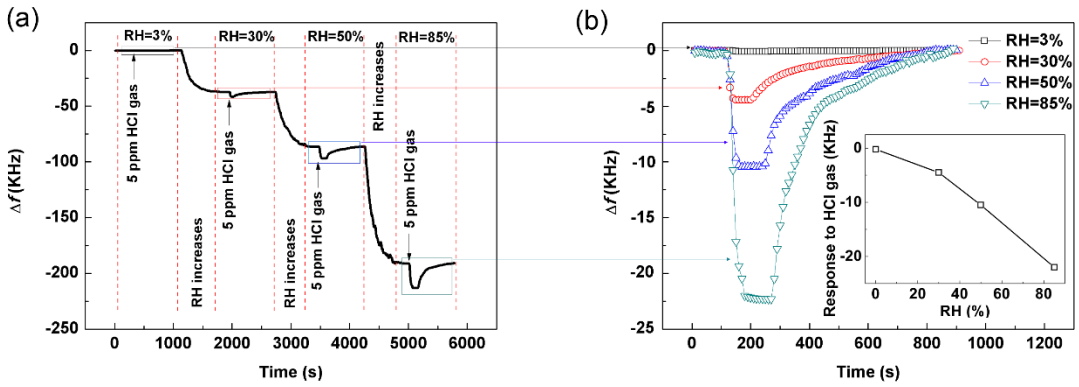

Figure 7 (a) Dynamic Responses of the sensor with CNCs-3 layer to 5 ppm HCl gas under different RH values and dynamic frequency shifts of the sensor when RH value changes; (b) Magnified pictures of the dynamic response processes in (a). Inset in (b) shows the response as a function of RH value.

Based on the above discussion, the SAW sensors with any hydrophilic layers may be sensitive to HCl gas. To verify this, sensors based on GO layer (~80 nm) and SiO_2 layer (~80 nm) were investigated and compared. FTIR results have confirmed that these two layers are also highly hydrophilic (Fig. 4). The responses of these two sensors to 5 ppm HCl at RH=3% and RH=50% are shown in Figs. 8(a) and 8(b). These two sensors also exhibit no significant responses to HCl at RH=3%, whereas show negative responses of -3.8 and -2.2 KHz, respectively, when the RH value is 50%. These responses are ~2.6 and ~4.5 times weaker compared with the response of the sensor coated with the CNCs-3 layer. This difference is mainly due to the different

amounts of H_2O molecules absorbed on different layers. As shown in Fig. 8 (a), the frequency shifts of the sensors coated with the GO and SiO_2 layers are -26.6 and -14.5 KHz when the ambient RH value is changed from 3% to 50%, these values are ~3.5 and ~6.6 times lower compared with those of coated with the CNCs-3 layer (Fig. 7(a)). These results clearly indicate that there are more H_2O molecules absorbed on the CNCs layer than those on SiO_2 and GO layers at RH=50%, which leads to stronger responses to HCl. With these results, it can be further confirmed that process (1) contributes mostly to the response of the sensor.

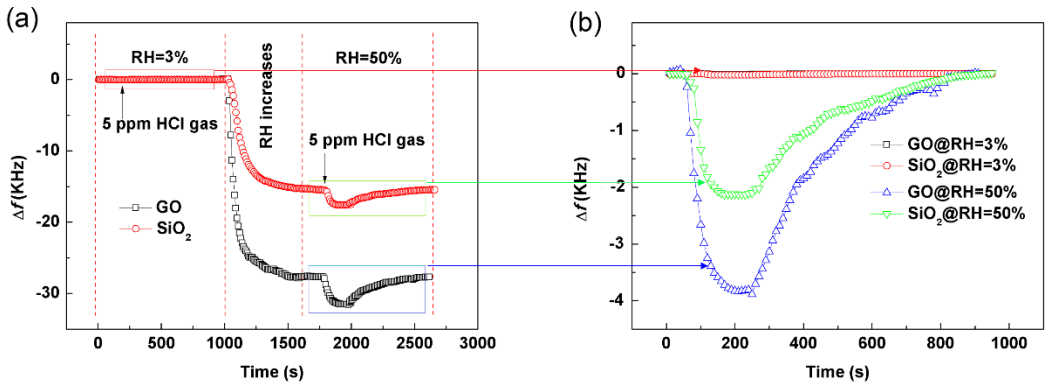

Figure 8 (a) Dynamic responses of the sensors with GO and SiO_2 layers to 5 ppm HCl gas under different RH values and dynamic frequency shifts of the sensors when RH value changes; (b) Magnified pictures of the dynamic response to HCl processes in (a).

The responses of this sensor to HCl gas of various concentrations were further investigated using the device of CNCs-3 at 25 °C and RH = 50%. As shown in Fig. 9(a), the sensor has an ability to detect HCl at a low concentration of 1 ppm with a response of -2 KHz, and the response can reach as high as -80 KHz when the concentration of HCl gas was increased to 200 ppm. Obviously, the response of the sensor shows a nonlinear relationship with the gas concentration as shown in Fig. 9(b). However, in the range from 1 to 20 ppm, the response is almost linear as a function of

the HCl concentration as shown in the inset picture in Fig. 9(b), indicating the good potentiality of the sensor for the practical application in detection of HCl gas with lower concentrations.

Fig. 9(c) shows the response and recovery times as a function of HCl gas concentration. Both of the response time and recovery time do not show significant changes when the concentration of the HCl gas is changed. The response of the sensor is fast, and the time is ~45 s, while the recovery time is relatively longer, which is ~500 s.

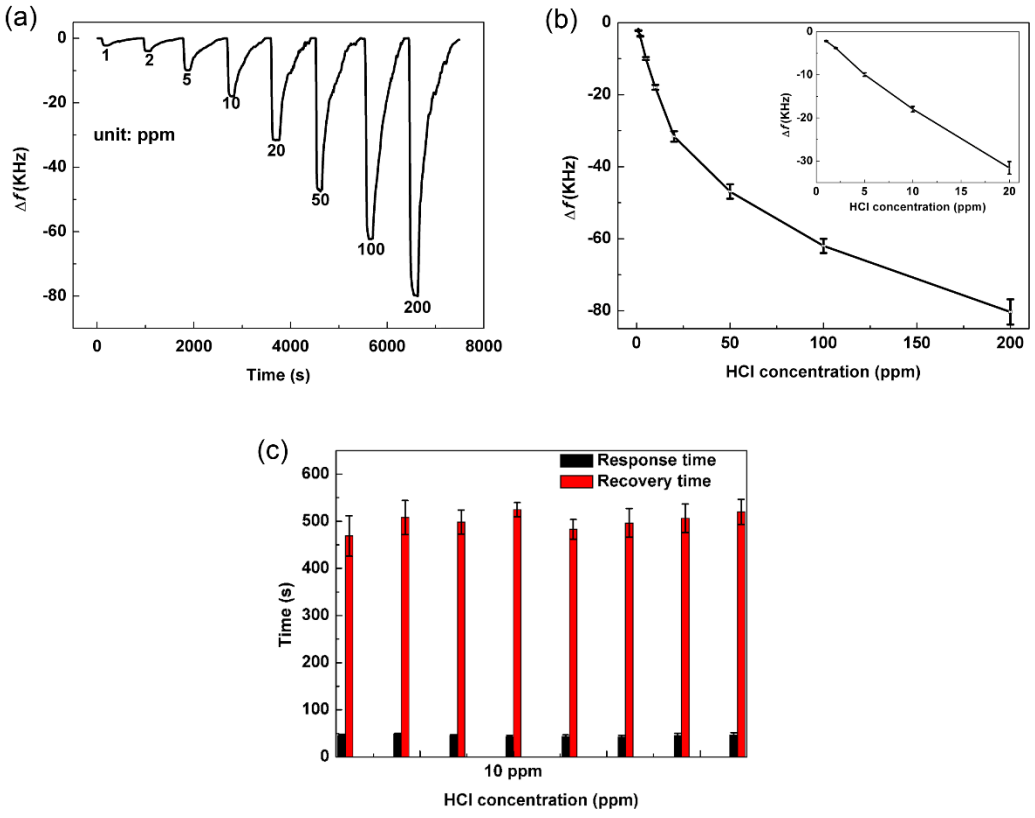

Figure 9 (a) Dynamic responses of the sensor with CNCs-3 layer to HCl gas with concentrations ranging from 1 to 200 ppm; (b) The responses as a function of HCl gas concentration. The inset picture gives the feature in the range from 1 to 20 ppm; (c)

The response and recovery times as functions of HCl gas concentration. All the data are acquired at 25 °C and RH=50%.

Based on the sensing mechanism discussed above, it can be assumed that the responses of the sensor are highly dependent on the solubility of the HCl gas in the H_2O. Fig. 10(a) presents the response of the sensor to different gases. Clearly the sensor shows no significant responses to gases with low solubilities in H_2O such as 50 ppm H_2, CO, CH_4 and H_2S, while it does show slight negative responses toward the gases with relative higher solubilities in H_2O such as 50 ppm SO_2 and NO_2. A slightly positive response to 50 ppm NH_3 gas, which has a quite high solubility in H_2O, can be also observed. Our previous report [49] has revealed that this response to NH_3 is a combination of two factors, i.e., a negative component caused by increase mass and a positive component derived from the condensation reactions between the hydrophilic groups catalyzed by the adsorbed NH_3. However, it is clear that the sensor's negative and positive responses to 50 ppm SO_2, NO_2 and NH_3 are much weaker than that to the 5 ppm HCl gas. This result indicates that the sensor has an excellent selectivity for HCl gas.

The reproducibility and short-term stability of the sensor were further investigated with exposing repeatedly the sensor to 5 ppm HCl for 4 cycles. As shown in Fig. 10(b), the sensor has similar response and recovery trends for each cycle, indicating good reproducibility and stability. The long-term stability of the sensor has also been investigated. As shown in Fig. 10(c), the sensor shows the similar responses to 1 ppm, 5ppm and 10 ppm HCl, respectively, in the 11 tests in 100 days, and the errors of these response are less than 5%, indicating its good long-term stability.

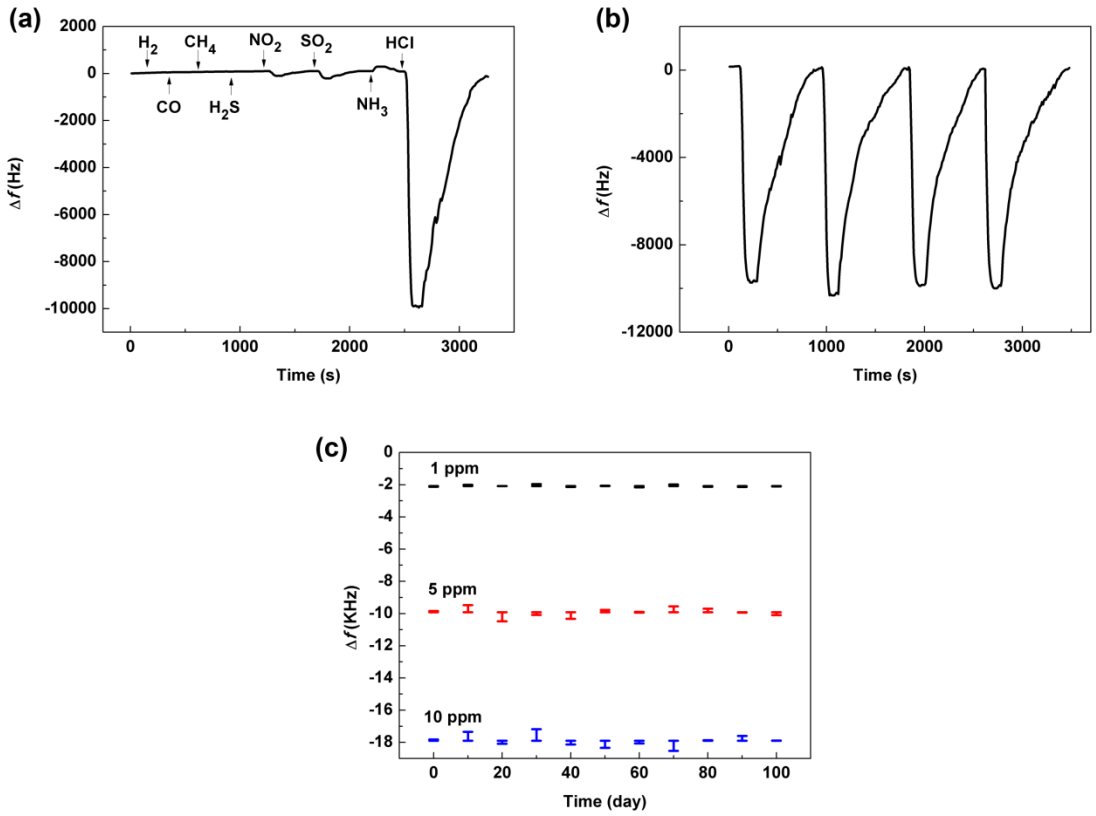

Figure 10 (a) Dynamic responses of the sensor with CNCs-3 layer to 50 ppm H_2, CO, CH_4, H_2S, SO_2, NO_2, NH_3 and 5 ppm HCl gases; (b) Dynamic responses of the sensor to 5 ppm HCl gas for 4 consecutive cycles; (c) The responses of the sensor to 1, 5 and 10 ppm HCl gases in 100 days. All the data are acquired at 25 °C and RH=50%.

4. Conclusion

In this article, SAW HCl gas sensors with the CNCs as the sensitive layers were fabricated and tested for their HCl sensing performance. The sensors can selectively detect HCl gas with a concentration as low as 1 ppm with a negative response of -2 kHz. This negative response was found to be caused by the increasing mass of sensitive layer, which is assisted by the H_2O absorbed on the sensitive layers. The sensing performance of the sensor is also highly influenced by thickness of sensing films and the ambient humidity because the amount of H_2O on the sensitive is highly dependent on these parameters. The sensor also exhibits excellent reproducibility and stability, indicating its good potentiality for practical applications.

Acknowledgement

This work was supported by the Fundamental Research Funds for the Central Universities (A0920502051904-67, A0920502051903-42), the Scientific Research Foundation of SWJTU (A1920502051907-2-032), the National Natural Science Foundation of China (11805158, 61178018) and the NSAF Joint Foundation of China (U1630126 and U1230124), and UK Engineering Physics and Science Research Council (EPSRC EP/P018998/1), Newton Mobility Grant (IE161019) through Royal Society and NFSC.

Reference

[1] F.J. Kelly, J.C. Fussell, Air pollution and public health: emerging hazards and improved understanding of risk, Environ. Geochem. Hlth. 37(2015) 631-649.

[2] T.J. Cova, P.E. Dennison, D. Li, F.A. Drews, L.K. Siebeneck, M.K. Lindell, Warning triggers in environmental hazards: who should be warned to do what and when?, Risk Anal. 37 (2017) 601-611.

[3] Z. Chen, J.N. Wang, G.X. Ma, Y.S. Zhang, China tackles the health effects of air pollution, Lancet 382 (2013) 1959-1960.

[4] R.B. Philp, Ecosystems and human health: toxicology and environmental hazards, Crc Press, 2013.

[5] J. Lelieveld, J.S. Evans, M. Fnais, D. Giannadaki, A. Pozzer, The contribution of outdoor air pollution sources to premature mortality on a global scale, Nature 525 (2015) 367.

[6] B. Brunekreef, S.T. Holgate, Air pollution and health, Lancet 360 (2002) 1233-1242.

[7] Y. Zhang, S. Yuan, X. Feng, H. Li, J. Zhou, B. Wang, Preparation of nanofibrous metal–organic framework filters for efficient air pollution control, J. Am. Chem. Soc. 138 (2016) 5785-5788.

[8] J.M. Samet, S. Gruskin, Air pollution, health, and human rights, Lancet Resp. Med. 3 (2015) 98-100.

[9] K. Wetchakun, T. Samerjai, N. Tamaekong, C. Liewhiran, C. Siriwong, V. Kruefu, A. Wisitsoraat, A. Tuantranont, S. Phanichphanta, Semiconducting metal oxides as

sensors for environmentally hazardous gases, Sens. Actuat. B-Chem. 160 (2011) 580-591.

[10] P.R. Shakya, P. Shrestha, C.S Tamrakar, P.K. Bhattarai, Studies on potential emission of hazardous gases due to uncontrolled open-air burning of waste vehicle tyres and their possible impacts on the environment, Atmos. Environ.42 (2008) 6555-6559.

[11] H. Wang, W.P. Lustig, J. Li, Sensing and capture of toxic and hazardous gases and vapors by metal–organic frameworks, Chem. Soc. Rev. 47 (2018) 4729-4756.

[12] M. Bal, T.T. Reddy, B.C. Meikap, Removal of HCl gas from off gases using self-priming venturi scrubber, J. Hazard. Mater. 364 (2019) 406-418.

[13] J. Li, Y.F. Zhou, Ocupational hazards control of hazardous substances in clean room of semiconductor manufacturing plant using CFD analysis, Toxicol. Ind. Health, 31(2015) 123-139.

[14] H. Zhang, S. Yu, L. Shao, P. He, Estimating source strengths of HCl and SO_2 emissions in the flue gas from waste incineration, J. Environ. Sci. 75 (2019) 370-377.

[15] E. Wang, K.F. Chow, W. Wang, C. Wong, C. Yee, A. Persad, J. Mann, A. Bocarsly, Optical sensing of HCl with phenol red doped sol–gels, Anal. Chim. Acta 534 (2005) 301-306.

[16] Y. Itagaki, K. Deki, S.I. Nakashima, Y.Sodaoka, Development of porphyrin dispersed sol–gel films as HCl sensitive optochemical gas sensor, Sens. Actuat. B-Chem. 117 (2006) 302-307.

[17] M. Cano, P. Castillero, J. Roales, J.M. Pedrosa, S. Brittle, T. Richardson, A.R. Gonzalez-Elipe, A. Barranco, A transparent TMPyP/TiO_2 composite thin film as an HCl sensitive optochemical gas sensor, Sens. Actuat. B-Chem.150 (2010) 764-769.

[18] H. Jeon, J. Lee, M.H. Kim, J. Yoon, Polydiacetylene-based electrospun fibers for detection of HCl gas, Macromol. Rapid Comm. 33 (2012) 972-976.

[19] M. Hu, W. Kang, B. Cheng, Z. Li, Y. Zhao, L. Li, Sensitive and fast optical HCl gas sensor using a nanoporous fiber membrane consisting of poly (lactic acid) doped with tetraphenylporphyrin, Microchim. Acta 183 (2016) 1713-1720.

[20] X. Wang, J. Wang, Y. Si, B. Ding, J. Yu, G. Sun, W. Luo, G. Zhang, Nanofiber-net-binary structured membranes for highly sensitive detection of trace HCl gas, Nanoscale 4 (2012) 7585-7592.

[21] C.W. Zhao, J.P. Ma, Q.K. Liu, X.R Wang, Y. Liu, J. Yang, J.S. Yang, Y.B. Dong, An in situ self-assembled Cu 4 I 4–MOF-based mixed matrix membrane: a highly sensitive and selective naked-eye sensor for gaseous HCl, Chem. Comm. 52 (2016) 5238-5241.

[22] M. Matsuguchi, Y. Kadowaki, Poly (acrylamide) derivatives for QCM-based HCl gas sensor applications, Sens. Actuat. B-Chem. 130 (2008) 842-847.

[23] M. Matsuguchi, N. Harada, S. Omori, Poly (N-isopropylacrylamide) nanoparticles for QCM-based gas sensing of HCl, Sens. Actuat. B-Chem. 190 (2014) 446-450.

[24] M. Matsuguchi, K. Takaoka, H. Kai, HCl gas adsorption/desorption properties of poly (N-isopropylacrylamide) brushes grafted onto quartz resonator for gas-sensing applications, Sens. Actuat. B-Chem. 208 (2015) 106-111.

[25] G. Gautschi, Piezoelectric sensors, Piezoelectric Sensorics, Springer, Berlin, Heidelberg, 2002 73-91.

[26] H.B. Lin, J.S. Shih, Fullerene C60-cryptand coated surface acoustic wave quartz crystal sensor for organic vapors, Sens. Actuat. B-Chem. 92 (2003) 243-254.

[27] T.M.A. Gronewold, Surface acoustic wave sensors in the bioanalytical field: Recent trends and challenges, Anal. Chim. Acta 603(2007) 119-128.

[28] W. Hao, J. Liu, M. Liu, Y. Liang, S. He, Mass sensitivity optimization of a surface acoustic wave sensor incorporating a resonator configuration, Sensors 16 (2016) 562.

[29] D.S. Ballantine, R.M. White R M, S.J. Martin, A.J. Ricco, E.T. Zellers, G.C. Frye, H. Wohltjen, Acoustic wave sensors: theory, design and physico-chemical applications, Elsevier, 1996.

[30] K. Bodenhöfer, A. Hierlemann, G. Noetzel, U. Weimar, W. Gopel, Performances of mass-sensitive devices for gas sensing: thickness shear mode and surface acoustic wave transducers. Anal. Chem. 68 (1996) 2210-2218.

[31] G. Siqueira, D. Kokkinis, R. Libanori, M.K. Hausmann, A.S. Gladman, A. Neels, P. Tingaut, T. Zimmermann, J.A. Lewis, A.R. Studart, Cellulose nanocrystal inks for 3D printing of textured cellular architectures, Adv. Funct. Mater. 27 (2017) 1604619.

[32] J. Tang, J. Sisler, N. Grishkewich, K.C. Tam, Functionalization of cellulose nanocrystals for advanced applications, J. Colloid Interf. Sci. 494 (2017) 397-409.

[33] X. Yang, K. Shi, I. Zhitomirsky, E.D. Cranston, Cellulose nanocrystal aerogels as universal 3D lightweight substrates for supercapacitor materials, Adv. Mater. 27 (2015) 6104-6109.

[34] W.J. Lee, A.J. Clancy, E. Kontturi, A. Bismark, M.S. Shaffer, Strong and stiff: high-performance cellulose nanocrystal/poly (vinyl alcohol) composite fibers, ACS Appl. Mater. Inter. 8 (2016) 31500-31504.

[35] D. Bagheriasl, P.J. Carreau, B. Riedl, C. Dubois, W.Y. Hamad, Shear rheology of polylactide (PLA)–cellulose nanocrystal (CNCS) nanocomposites, Cellulose 23 (2016) 1885-1897.

[36] N. Grishkewich, N. Mohammed, J. Tang, K.C. Tam, Recent advances in the application of cellulose nanocrystals, Curr. Opin. Colloid In. 29 (2017) 32-45.

[37] H. Golmohammadi, E. Morales-Narvaez, T. Naghdi, M. Arben, Nanocellulose in sensing and biosensing, Chem. Mater. 29 (2017) 5426-5446.

[38] E. Kontturi, A. Meriluoto, P.A. Penttilä, N. Baccile, J.M. Malho, A. Potthast, T. Rosenau, J. Ruokolainen, R. Serimaa, J. Laine, H. Sixta, Degradation and crystallization of cellulose in hydrogen chloride vapor for high-yield isolation of cellulose nanocrystals, Angew.Chem.Inter. Edit. 55 (2016) 14455-14458.

[39] E. Kloser, D.G. Gray, Surface grafting of cellulose nanocrystals with poly (ethylene oxide) in aqueous media, Langmuir 26 (2010) 13450-13456.

[40] P. Lu, Y.L. Hsieh, Preparation and properties of cellulose nanocrystals: rods, spheres, and network, Carbohyd. Polym. 82 (2010) 329-336.

[41] Y. Tang, Z. Li, J. Ma, W. Lu, J. Yang, B. DU, Q. Yu, X. Zu, Highly sensitive surface acoustic wave (SAW) humidity sensors based on sol–gel SiO_2 films: Investigations on the sensing property and mechanism, Sens. Actuat. B-Chem. 215 (2015) 283-291.

[42] Cheng G, Varanasi P, Li C, H. Liu, Y.B. Melnichenko, B.A. Simmons, M.S. Kent, S. Singh, Transition of cellulose crystalline structure and surface morphology of biomass as a function of ionic liquid pretreatment and its relation to enzymatic hydrolysis, Biomacromolecules 12 (2011) 933-941.

[43] L. Segal, J.J. Creely, A.E. Martin, C.M. Cornad, An empirical method for estimating the degree of crystallinity of native cellulose using the X-ray diffractometer, Text. Res. J. 29 (1959) 786-794.

[44] G.M. Doris, D.G. Gray, The surface analysis of paper and wood fibers by ESCA. I. Cell. Chem. and Technol. 12 (1978) 9-23.

[45] Y. Gao, X.H. Wang, H.P. Yang, H.P. Chen, Characterization of products from hydrothermal treatments of cellulose, Energy 42 (2012) 457-465.

[46] V.B. Raj, H. Singh, A.T. Nimal, M.U. Sharma, M. Tomar, V. Gupta, Distinct detection of liquor ammonia by ZnO/SAW sensor: study of complete sensing mechanism, Sensor. Actuat. B-Chem. 238 (2017) 83-90.

[47] D.S. Ballantine Jr., S.J. Martin, A.J. Ricco, G.C. Frye, H. Wohltjen, R.M. White, E.T. Zellers, Acoustic Wave Sensors: Theory, Design, and Physico-Chemical Applications, Academic Press, San Diego, 1997.

[48] M. Thompson, D.C. Stone, Surface-launched acoustic wave sensors: chemical sensing and thin-film characterization, Wiley-Interscience, 1997.

[49] Y. Tang, D. Ao, W. Li, X. Zu, S. Li, Y.Q. Fu, NH_3 sensing property and mechanisms of quartz surface acoustic wave sensors deposited with SiO_2, TiO_2, and SiO_2-TiO_2 composite films, Sens.Actuat. B-Chem. 254 (2018) 1165-1173.